Asian Journal of Chemistry; Vol. 31, No. 10 (2019), 2311-2318

ASIAN JOURNAL OF CHEMISTRY

https://doi.org/10.14233/ajchem.2019.22162

Design, Synthesis, Characterization and Antiproliferative Activities of Ru(II) Complexes of Substituted Benzimidazoles

ASHOK K. SINGH[1,*], SNEHLATA KATHERIA[1], AMRENDRA KUMAR[2], ASIFF ZAFRI[3] and MOHD. ARSHAD[3]

[1]Department of Chemistry, University of Lucknow, Lucknow-226007, India
[2]Department of Physics, University of Lucknow, Lucknow-226007, India
[3]Department of Zoology, University of Lucknow, Lucknow-226007, India

*Corresponding author: E-mail: singhaks3@rediffmail.com

Received: 29 April 2019; *Accepted*: 31 May 2019; *Published online*: 30 August 2019; AJC-19542

Synthesis of $[Ru(PPh_3)_2(BZM)_2Cl_2]$ (BZM= LS1, LS2, LS3, LS4 and LS5) where LS1 = (1*H*-benzo[*d*]imidazole-2-yl)methanethiol, LS2 = 2-(4-bromobutyl)-1*H*-benzo[*d*]imidazole, LS3 = 2-(4-nitrophenyl)-1*H*-benzo[*d*]imidazole, LS4 = 2-(4-chlorophenyl)-1*H*-benzo[*d*]imidazole and LS5= 4-(1*H*-benzo[*d*]imidazol-2-yl)aniline (BZM = benzimidazoles, PPh_3 = triphenylphosphine) and metal complexes as MR, $[Ru(PPh_3)_4Cl_2]$, MLS1, MLS2, MLS3, MLS4 and MLS5 for use as potential anticancer compounds have been investigated. The complexes have been characterized by elemental analysis, IR, multinuclear NMR, UV-visible and ESI-MS spectroscopic techniques. The geometries of all complexes have been optimized by using density functional theory (DFT). The cytotoxicity effects of MR, MLS2 and LS1 were also investigated on Human cervical carcinoma cells (HeLa) by MTT assay, ROS generation and nuclear apoptosis assay. The percent cell viability assessed by MTT assay suggested that the synthesized MR, MLS2 and LS1 significantly reduce the viability of HeLa cells, in a dose-dependent manner. The inhibitory concentration (IC_{50}) of MR, MLS2 and LS1 against HeLa cells was found 90.8, 81.8 and 115 μM, respectively. These compounds also induced the over production of intracellular reactive oxygen species (ROS) as well as the condensed and fragmented nucleus, which supports the molecular mechanism of cell death by apoptosis. The investigations suggested that the compounds MR, MLS2 and LS1 induce the cell death in HeLa cells through apoptotic pathway.

Keywords: Ruthenium(II) complex, Benzimidazoles, Apoptosis, Cytotoxicity effect.

INTRODUCTION

Platinum complexes attracted researcher's interests due to its promising anticancer properties, because they are still the most successful medical therapeutic metallodrugs [1,2]. Due to the serious side effects of platinum drugs, we encouraged the development of anticancer agents on the basis of other metals with low side effects. In this direction, ruthenium compounds also represent a promising metal-based anticancer complex that can offer less toxicity than platinum based drugs [3]. It demonstrated some exciting antitumor properties and this may be the alternative option to platinum based antitumor medicines. Additionally, ruthenium has the ability to mimic iron cation binding to certain molecules, in view of rate of ligand exchange and accessible oxidation states [4]. Further, imidazole ligand shows imperative role with ruthenium to target site recognition against ovarian carcinoma cells [5]. In particular, some ruthenium derivative have been screened for their antineoplastic activity and their derivative $[H_2Im][$*trans*-$Ru(III)Cl_4(DMSO\text{-}S)(HIm)]$ (NAMI-A) and imidazolium *trans*-[transchlorobis(1*H*-indazole)-ruthenate(III)] (KP1019 or FFC14A) were the first ruthenium based anticancer complexes that have been entered into clinical trials [6,7]. Further, the ruthenium complexes comprising of chalcones and flavones will be possible drugs against breast cancer [8,9]. Since the toxicity of many drugs used in chemotherapy limits their clinical sources, subsequently analyzed the cytotoxic activity of the compounds using MTT assay [10].

The potential of different metal based anticancer agent have been widely explored and especially ruthenium complexes have been extensively studied in drug discovery [11]. The drug resistance developed by cisplatin against cancer cells, have led to new line of approach for development of new ruthenium

complexes for metal based drug that can be used in the fields of chemotherapy. In general, the drug discovery approach targets the DNA or cellular mechanism [12]. Therefore, the interaction of ruthenium complexes to adenine, guanine and cytosine, through weak interaction and hydrogen bonding, signifying the possibility to design compounds to interact through nucleotides [12]. The binding modes and affinity of ruthenium complexes also depends on the structure of DNA [13]. In this respect, we have synthesized ruthenium complexes containing a triphenylphosphine and substituted benzimidazole and assessed their interaction with human cervical carcinoma cells. The cytotoxicity of the complexes was assessed using cancer and normal cell lines *in vitro* conditions.

EXPERIMENTAL

The reagent and chemicals used for synthesis were procured from Sigma Aldrich, Hi-media and Merck and used without further purification. Column chromatography of all the synthesized compounds was performed by silica gel 60 (40-60 Merck, India) as stationary phase and acetonitrile as an eluent. FT-IR spectra were recorded in KBr pellets on Perkin Elmer AC-1C spectrometer from 4000 to 450 cm^{-1}. ^1H NMR spectra were recorded in DMSO-d_6 on Bruker Avance III HD spectrometer at 300 MHz using TMS as an internal reference. ESI-MS mass spectra were recorded on JEOL SX 102/DA-6000 spectrometer. Elemental analysis was performed on Exeter analytical INC Model CE-440 C H N ANALYSER. Electronic absorption spectra were recorded on Labtronic 2900 UV-Vis spectrophotometer and conductivity is carried out on microprocessor based conductivity/TDS meter ESICO Model 1601.

in vitro Cytotoxicity activity studies

Cervical carcinoma cell line (HeLa) culture: The cell line of human cervix carcinoma (HeLa) was procured from the National Centre for Cell Sciences (NCCS), Pune, India. The cell was cultured at 37 ºC humidified condition and 5 % CO_2 in MEM (E) culture media. The medium was supplemented with 10 % fetal bovine serum (FBS), 1 % antibiotic solution (10,000 U/mL penicillin and 10 mg/mL streptomycin), 0.1 mM non-essential amino acids, 2.0 mM L-glutamine, 1.0 mM sodium pyruvate and 1.5 g/L $NaHCO_3$.

Cell viability assay on HeLa cells: HeLa cells (1×10^4 cells per mL) were seeded in 100 µL MEM (E) media per well in 96 well titer plate for 24 h at 37 ºC and 5 % CO_2 as per previous protocol [13]. The treatment was conducted for 24 h incubation with various concentrations (10, 25, 50, 100 and 200 µM) of the MR, MLS2 and LS1. Afterwards, 20 µL of MTT reagent was added to each well and kept for 4 h at 37 ºC until the development of formazan crystals. Subsequently, the obtained formazan crystals were solubilized in 100 µL of DMSO and the absorbance was recorded at 540 nm using a microplate reader (BIORAD-680). The % cell viability has been presented as a ratio of absorbance of treated groups to the absorbance of control cells (without treatment). The % cell viability was calculated following the given equation:

$$\text{Cell viability (\%)} = \frac{A_{540}\ \text{(treated cells)}}{A_{540}\ \text{(control cells)}} \times 100$$

Cellular morphology studies in HeLa cells: The morphological changes in HeLa cells, treated with MR, MLS2 and LS1 were examined under the inverted contrast-phase microscope. Briefly, HeLa cells was plated in 48 well culture plates and treated with 10, 25, 50, 100 and 200 µM concentrations of MR, MLS2 and LS1 for 24 h of incubation. Thereafter, the cell morphology was examined by an inverted contrast-phase microscope and photographed [14].

Detection of ROS in HeLa cells: The intracellular ROS level was detected by DCFH-DA (2,7-dichlorodihydrofluoresce in diacetate) staining in accordance with the previous report [15]. The HeLa cells were first seeded at the density 1×10^4 per well in a 96-well culture plate and incubated at 37 ºC for 24 h in 5 % CO_2. Then, cells were exposed to 25, 50 and 100 µM concentrations of MR, MLS2 and LS1 for 12 h. Subsequently, for the fluorescence microscopy imaging, the cells were washed thrice with PBS (phosphate buffer saline) and then incubated with fluorescence agent DCFH-DA (10 mM) for 25 min at 37 ºC. Later, cells were washed with MEM (E) three times and were observed with a fluorescence inverted microscope (Nikon ECLIPSE Ti-S, Japan). For the quantitative analysis of ROS, HeLa cells (1×10^4 per well) were seeded in 96-well black bottom titer plate and treated with 25, 50 and 100 µM concentrations of the MR, MLS2 and LS1. Afterwards, cells were trypsinized and washed thrice with PBS, then incubated with DCFH-DA (10 mM) for 25 min. The cells were analyzed for the fluorescence intensity by a multiwall microplate reader (Synergy, BioTek) with an excitation and emission wavelength at 485 and 528 nm, respectively. The values of fluorescence intensity were expressed as the percentage of the treated group with respect to the control group.

Analysis of nuclear apoptosis in HeLa cells: For the nuclear and chromatin structural change study, the HeLa cells were seeded in 96 well culture plate and then treated with different doses of MR, MLS2 and LS1 at 25, 50 and 100 µM concentrations for 24 h [16]. Consequently, cells were washed thrice with PBS and fixed in 4 % paraformaldehyde (used as a fixative) for 10 min and then permeabilized with permeabilizing buffer (4 % paraformaldehyde and 0.5 % Triton X-100) and stained with 10 mM of DAPI stain. After staining, cells were examined with the help of an inverted fluorescence microscope at the excitation wavelength of 360 nm and an emission wavelength of 454 nm (Nikon ECLIPSE Ti-S, Japan) [16]. For the quantitative analysis of apoptotic cells, the tests were performed thrice for every treatment group and the 100 cells per well were calculated in at least 10 random fields per well, to count the percent apoptotic cells using an inverted fluorescent microscope (Nikon ECLIPSE Ti-S, Japan).

Statistical analysis: The data on cell viability, nuclear condensation and ROS generation were represented as mean ± standard error mean (SEM) from at least three independent studies. Determination of difference in between the experimental and the control groups was compared using one-way ANOVA followed by Dunnett's multiple range test of Graph Pad prism software (Version 5.01). The p value of less than 0.05 was designated to be statistically significant.

General procedure for synthesis of ligands (LS1-LS5): All substituted benzimidazole ligands were prepared by the

previously reported procedure [17]. *o*-Phenylenediamine (0.25 mol) and appropriate carboxylic acid (0.34 mol) was heated on an oil bath at 100 ºC for 8 h. The completion of the reaction was monitored by TLC. After completion of the reaction, the reaction mixture was cooled and its pH was adjusted between 7-8 using 10% NaOH solution. The crude benzimidazole was filtered and washed with ice-cold water. The crude product was dissolved in 40 mL of boiling water and 2 g of carbon was added and digested for 15 min. The solution was filtered while hot, cooled the filtrate to about 10 ºC. The pure product obtained was filtered, washed with 25 mL of cold water and dried (**Scheme-I**).

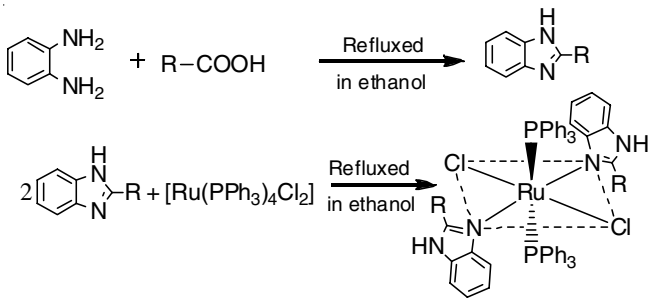

R = SH (LS1), Br (LS2), NO_2 (LS3), Cl (LS4), NH_2 (LS5)

Scheme-I: Synthetic route for synthesis of ligand and its ruthenium(II) complexes

(1*H*-Benzo[*d*]imidazole-2-yl) methanethiol (LS1): Pale yellow solid; yield: 42.90 %, m.p.: 158 ºC, IR (KBr, ν_{max}, cm^{-1}): 3445 (N-H *str.*), 2963 (Ar C-H), 2600 (S-H *str.*), 1700 (Ar-C), 1600 (C=N), 2900 (Ar C-H). ^{1}H NMR (300 MHz, DMSO-d_6, δ ppm): δ 7.01-7.51 (m, 4H Ar-H), 4.41 (s, 1H, N-H), 2.01 (s, 2H, CH_2), 2.2(s 1H, SH). ^{13}C NMR (300 MHz, DMSO-d_6, δ ppm): 133, 132, 122, UV-Vis (DMSO, λ_{max}, nm ($\varepsilon_{max} \times 10^3$ M^{-1} cm^{-1}): 250 (2.2), 300 (2.4), 348 (0.1).

2-(4-Bromobutyl)-1*H*-benzo[*d*]imidazole (LS2): Reddish brown solid; yield: 40.4 %, m.p.: 166 ºC, IR (KBr, ν_{max}, cm^{-1}): 3300 (N-H *str.*), 1527(C=N *str.*), 2900(ArH, C-H), 1700 (Ar C=C). ^{1}H NMR (300 MHz, DMSO-d_6, δ ppm): δ 6.57-7.90 (m, 8H, Ar-H), 6.96 (s, 1H, N-H), 2.50-2.54 (m, 8H, CH_2); ^{13}C NMR (300 MHz, DMSO-d_6, δ ppm): δ 146, 142, 141, 136, 133, 128, 126, 123, 121, 118, 115, 101. UV-Vis (DMSO, λ_{max}, nm ($\varepsilon_{max} \times 10^3$ M^{-1} cm^{-1}): 240 (0.9), 270 (0.95), 275 (0.8).

2-(4-Nitrophenyl)-1*H*-benzo[*d*]imidazole (LS3): Brown solid ; yield: 40.50 %, m.p.: 220 ºC, IR (KBr, ν_{max}, cm^{-1}): 3100 (N-H *str.*), 3000 (Ar C-H), 1350 (N-O sym *str.*), 1400 (C-N *str.*), (C-Br), 1700 (C=C ring *str.*), 1602 (N-O asym *str.*), 1539 (C=N *str.*). ^{1}H NMR (300 MHz, DMSO-d_6, δ ppm): δ 7.57-8.22 (m, 8H, Ar-H), 6.87 (s, 1H , N-H). ^{13}C NMR (300 MHz, DMSO-d_6, δ ppm): δ 167, 150, 146, 141, 138, 137, 131, 128, 126, 124, 101. UV-Vis (DMSO, λ_{max}, nm ($\varepsilon_{max} \times 10^3$ M^{-1} cm^{-1}): 250 (1.7), 340 (0.1), 450 (0.5).

2-(4-Chlorophenyl)-1*H*-benzo[*d*]imidazole (LS4): Black colour solid; yield: 39.6 %, m.p. 234 ºC, IR (KBr, ν_{max}, cm^{-1}): 3150(NH *str.*), 3000 (ArH), (C-Cl),1525 (C=N),1600 (C=C ring system), 1429 (C-N *str.*). ^{1}H NMR (300 MHz, DMSO-d_6, δ ppm): δ 7.52-8.12 (m, 8H, Ar-H), 6.80 (s,1H N-H). ^{13}C NMR (300 MHz, DMSO-d_6, δ ppm): δ 165, 149, 145, 141, 138, 130, 128, 126, 123, 101. UV-Vis (DMSO, λ_{max}, nm ($\varepsilon_{max} \times 10^3$ M^{-1} cm^{-1}): 270 (2.4), 360 (0.1), 420 (4.0).

4-(1*H*-Benzo[*d*]imidazol-2-yl)aniline (LS5): Brown colour solid; yield: 42.6 %; m.p.: 226 º, IR (KBr, ν_{max}, cm^{-1}) 3600 (N-H *str.*), 1450 (C=N *str.*), 1650 (Ar-C=C), 2350 (Ar N-H(NH_2)), 2900 (Ar C-H), 850 (Ar C-N). ^{1}H NMR (300 MHz, DMSO-d_6, δ ppm): δ 6.40-7.89 (m, 8H, Ar-H), 6.40 (s, 1H, N-H), 2.50 (s, 2H, NH_2). ^{13}C NMR (300 MHz, DMSO-d_6, δ ppm): δ 145, 142, 139, 128, 127, 102. UV-Vis (DMSO, λ_{max}, nm ($\varepsilon_{max} \times 10^3$ M^{-1} cm^{-1}): 320 (0.5), 420 (4.0).

General procedure for synthesis of Ru(II) complexes: The ruthenium precursor was prepared in accordance with the previously reported method [18]. The precursor was synthesized with the reaction of ruthenium trichloride trihydrate with a methanolic solution of tryphinylphosphine in excess and refluxed for 8 h under nitrogen,which gives the black precipitate of $[RuCl_2(PPh_3)_4]$ (**MR**), washed with diethylether and dried *in vaccuo*. Triphenylphosphine ligands are easily replaced by other ligands in the precursor complexes [19]. The complexes of general formula $[Ru(PPh_3)_2(BZM)_2Cl_2]$ were synthesized by the reaction of ruthenium dichlorotetratriphenylphosphine with different substituted benzimidazole in 1:2 molar ratio in methanol. Further, $RuCl_2(pph_3)_4$ (0.265 g, 1 mmol) was added to a methanolic solution of the ligands, 2 mmol (**LS1**, 0.328g; **LS2**, 0.554 g; **LS3**, 0.478 g; **LS4**, 0.146 g; **LS5**, 0.456 g). The solutions were refluxed for 10 h in nitrogen and reduced the volume, thus a microcrystalline precipitate was obtained (**Scheme-I**). The analytical data for these complexes are in good agreement with their respective molecular formula. The new complexes were formed by the substitution of two triphenyl phosphine complexes by benzimidazole which indicates the labile nature of phosphine bond and addition of Nitrogen based ligands, this is due to the better sigma (σ) donating ability of the nitrogen bases to that of triphenylphosphine [20]. The complexes were sparingly soluble in organic solvent as acetone, alcohol and methanol but soluble in DMSO/DMF. The molar conductivities values were 0.055-0.163 ohm^{-1} cm^2 mol^{-1}. The observed values indicates the non-electrolytic nature of complexes.

$[Ru(PPh_3)_2(LS1)_2Cl_2]\cdot 3H_2O$ (MLS1): Dark brown colour, yield: 46 %; m.p.: 327 ºC, IR (KBr, ν_{max}, cm^{-1}): 1143 (P-Ph), 1328 ν(-NH), 2963 (NH), ^{1}H NMR (300 MHz, DMSO-d_6, δ ppm): δ 6.80 (m, PPh_3), 7.01-7.66 (m, 4H, Ar-H), 4.01 (s, 1H, NH), 2.40 (2H, CH_2); 2.49 (s, 1H, sh); ^{13}C NMR (300 MHz, DMSO-d_6, δ ppm): δ 135, 122; MS (ESI) *m/z*: 1077 (1076). Anal. calcd. (found) (%) $RuP_2C_{12}C_{52}H_{52}N_4S_2O_3$: C, 57.09 (57.09); H, 4.83 (4.83); N, 5.20 (4.80). ^{31}P NMR (500 MHz, DMSO-d_6, δ ppm): δ 40.34 ppm (s, PPh_3). UV-Vis (DMSO, λ_{max}, nm ($\varepsilon_{max} \times 10^3$ M^{-1} cm^{-1}): 240 (3.5), 260 (3.2), 450 (1.0).

$[Ru(PPh_3)_2Cl_2(LS2)_2]$ (MLS2): Dark red colour: yield: 62 %; m.p.: 296 ºC, IR (KBr, ν_{max}, cm^{-1}): 1156 (P-Ph), 1371 (NH_2), 3056 (NH_2 *str.*), ^{1}H NMR (300 MHz, DMSO-d_6, δ ppm): δ 6.67 (s, PPh_3), 7.26-7.66 (m, 8H, Ar-H), 6.60 (2H, NH), 1.25-3.79 (m,16H,CH_2). ^{13}C NMR (300 MHz, DMSO-d_6, δ ppm): δ 134, 133, 132, 131, 129, 128. ESI-MS *m/z*: 1177 (1178). Anal. calcd. (found) (%) $RuP_2Cl_2C_{56}H_{56}N_4Br_2$: C, 57.09 (56.59); H, 4.75 (4.25); N, 4.75 (4.55). ^{31}P NMR (500 MHz, DMSO-d_6, δ ppm): δ 40.38. UV-Vis (DMSO, λ_{max}, nm ($\varepsilon_{max} \times 10^3$ M^{-1} cm^{-1}): 240 (2.53), 260 (0.6), 450 (1.0).

$[Ru(PPh_3)_2Cl_2(LS3)_2]H_2O$ (MLS3): Brownish, yield: 42 %; m.p.: 320 ºC, IR (KBr, ν_{max}, cm^{-1}): 1171 (PPh), 1585 (C=N),

1926 (NO), ^{1}H NMR (300 MHz, DMSO-d_6, δ ppm): 6.90 (s, PPh_3), 7.56-8.26 (16H, Ar-H), 6.60 (2H, NH). ^{13}C NMR (300 MHz, DMSO-d_6, δ ppm): 166, 150, 145, 141, 138, 136, 131, 127, 127, 124, 101. ESI-MS *m/z*: 1191 (1192). Anal. calcd. (found) (%) $RuP_2Cl_2C_{62}H_{50}N_6O_5$: C, 62.46 (62.92); H, 4.19 (4.16); N, 7.16 (6.66). ^{31}P NMR (500 MHz, DMSO-d_6, δ ppm): δ 40.53. UV-Vis (DMSO, λ_{max}, nm ($\varepsilon_{max} \times 10^3$ M^{-1} cm^{-1}): 220 (2.6), 260 (2.65), 275 (2.4), 350 (1.8), 450 (0.5).

$[Ru(PPh_3)_2(LS4)_2Cl_2]\cdot H_2O$ (MLS4): Black, yield: 42 %, m.p.: 308 ºC, IR (KBr, ν_{max}, cm^{-1}): 1199 (P-Ph), 1320 (NH_2), 3700 (NH_2 *str.*), ^{1}H NMR (300 MHz, DMSO-d_6, δ ppm): 7.13 (m, PPh_3), 7.28-8.04 (m, ArH), 6.80 (s, NH), ^{13}C NMR (300 MHz, DMSO-d_6, δ ppm): 168, 137, 135, 133, 132, 131, 129, 128, 121, ESI-MS *m/z*: 1099 (1100). Anal. calcd. (found) (%) $RuP_2Cl_2C_{62}H_{50}N_4O$: C, 67.69 (67.09); H, 4.54 (4.04); N, 0.36 (0.26). ^{31}P NMR (500 MHz, DMSO-d_6, δ ppm): 40.54, UV-Vis (DMSO, λ_{max}, nm ($\varepsilon_{max} \times 10^3$ M^{-1} cm^{-1}): 240 (2.5), 255 (0.6), 450 (0.5), 550 (0.8).

$[Ru(PPh_3)_2(LS5)_2Cl_2]\cdot 2H_2O$ (MLS5): Black crystalline colour: yield: 38 %, m.p.: 348 ºC, IR (KBr, ν_{max}, cm^{-1}): 1186 (P-Ph), 1314 (NH_2), 3300 (NH_2 *str.*); ^{1}H NMR (300 MHz, DMSO-d_6, δ ppm): 6.91 (m, PPh_3), 7.54-7.90 (m, ArH), 2.50 (s, 2H, NH_2), 6.42 (s, H, NH), ^{13}C NMR (300 MHz, DMSO-d_6, δ ppm): 144, 142, 139, 127, 101. ESI-MS m/z: 1149 (1151). Anal. calcd. (found) (%): C, 64.75 (64.25); H, 4.87 (4.07); N, 7.31 (7.01). ^{31}P NMR (500 MHz, DMSO-d_6, δ ppm): 40.58. UV-Vis (DMSO, λ_{max}, nm ($\varepsilon_{max} \times 10^3$ M^{-1} cm^{-1}): 250 (3.3), 405 (2.3), 460 (1.5).

Computational details: The Gaussion-09 program package was used to perform density functional theory (DFT) calculations [21]. The gas phase geometry of complexes were fully optimized using B3LYP hybrid functional using 6-31G** basis set for all the atoms expect Ru. For Ru, LANL2DZ basis set was used [22,23].

RESULTS AND DISCUSSION

Infrared studies: Infrared spectra of the ligands showed the characteristic band at 1600-1450 and 3600-3100 cm^{-1} which corresponds to ν(C=N) and ν(N-H) for **LS1-LS5**. The vibrational spectra of the metal complexes were compared with the corresponding ligands to study the binding behaviour of ruthenium metal to the ligand. The band position of metal complexes at 3145 cm^{-1} was observed in all the cases which could be assigned to ν(N-H) of benzimidazole. This feature suggested that the group NH is not coordinated nor deprotonated during complex formation. Though, there was shift in ν(C=N) in the spectra of the complexes containing benzimidazole, suggests coordination of ruthenium metal ion through nitrogen. Further, in all complexes, band position in the range 1199-1143 of M-PPh_3 suggests the coordination of metal-phosphorus [24].

NMR studies: The ^{1}H NMR spectra, display aromatic protons in the range, δ 8.0-6.0 ppm in all complexes and there integration indicates the coordination of two benzimidazole moiety. In **MLS1**, two multiplet in the range δ 7.23-7.26 and proton signals at δ 6.52 (4H) and singlet at δ 4.0 (2H) indicated the presence of amino phenyl group. In **MLS2**, ^{1}H NMR spectrum showed a singlet at δ 1.5(2H) and δ 3.82 (3H) protons confirmed the presence of methane thiol group. In **MLS3**, multiplet at δ 3.12 for one proton and doublet at δ 1.29 for six protons indicate the presence of propane group. In case of **MLS4**, two multiplets at δ 8.25 and δ 7.74 for two protons indicated the substitution of nitro phenyl at C2 of benzimidazole nucleus. One weak singlet at δ 12.40 may be assigned to the N-H proton of benzimidazole.

^{31}P spectra of all the ruthenium(II) complexes were recorded in DMSO-d_6 in order to confirm the presence of triphenyl phosphine groups and to determine the geometry of the complexes. The observation of sharp singlet peak in the range δ 7.50-6.40, suggest the only one possible geometric isomer of the complexes is formed [25]. However, IR spectrum showed single absorption band around 1199-1143 cm^{-1}, suggests that triphenyphosphine is in *trans*-position [26].

Electronic absorption spectroscopy: The UV-visible absorption spectral assignments of complexes are presented in Table-1. The intense high energy band below 300 nm is assigned to ligand centered transitions. The low energy absorptions at 600 nm arise due to Ru based MLCT transitions. The nature of the observed electronic spectra and the positions of absorption band are consistent with those of other similar octahedral Ru(II) complexes [27]. Further, all ruthenium complexes are found to be diamagnetic which suggest that their geometry ought to be octahedral as revealed by geometry optimization. The absorption band in the range 220-450 nm, based on the values of extinction coefficient (2.2-0.50) both band assigned to π-π^* transitions arising from an excitation of an intra ligand orbitals.

TABLE-1
UV-VISIBLE SPECTRAL DATA OF THE LIGANDS AND Ru(II) COMPLEXES IN METHANOL

Compounds	Λ_{max} (nm) ($\varepsilon_{max} \times 10^3$ M^{-1} cm^{-1})
LS1	244 (0.17), 230 (0.34), 2390.61), 250 (1.05), 258 (1.14), 260 (1.15), 265 (1.12), 270 (1.10), 277 (1.10), 280 (1.09), 283 (0.01)
LS2	213 (1.45), 244 (1.42), 251 (1.66), 267 (1.69), 279 (1.42), 293 (0.14), 3469 (0.01), 441 (0.52)
LS3	236 (1.92), 241 (2.02), 249 (2.28), 258 (2.39), 265 (2.29), 281 (2.31), 291 (2.43), 295 (2.36), 326 (0.26), 341 (0.19), 347 (0.17)
LS4	212 (0.72), 230 (0.73), 240 (1.51), 253 (1.42), 267 (1.37), 273 (1.48), 275 (1.11), 279 (1.18)
LS5	227 (1.79), 231 (1.92), 243 (2.23), 247 (2.38), 252 (2.48), 260 (2.42) 265 (2.43), 269 (2.38), 280 (2.41), 299 (2.53), 310 (2.20), 332 (2.20), 429 (0.63)
MLS1	213 (1.15), 223 (1.60), 230 (2.04), 234 (2.15), 250 (2.50), 257 (2.90), 272 (2.96), 279 (2.90), 301, 339 (1.50), 350 (2.15), 359 (2.00), 363 (0.75), 399 (0.59)
MLS2	209 (0.39), 221 (0.29), 229 (0.30), 259 (0.53), 277 (0.33), 300 (0.22), 340 (0.12), 400 (0.17), 420 (0.20), 460 (0.20), 500 (0.06)
MLS3	205 (0.60), 213 (1.53), 217 (1.51), 223 (2.03), 226 (2.13), 238 (1.30), 255 (0.75), 268 (0.76), 287 (0.45), 449 (0.35), 540 (0.51), 601 (0.35), 652 (0.25), 703 (0.16)
MLS4	212 (0.73), 230 (0.78), 240 (1.49), 250 (1.49), 267 (1.37), 273 (1.50), 324, 357, 372
MLS5	215 (2.20), 223 (2.36), 230 (2.64), 248 (2.67), 256 (2.90), 263 (2.07), 273 (2.96), 281 (3.01), 294 (3.01), 309 (1.96), 338 (2.11), 350 (2.15), 354 (2.27), 359 (2.59), 363 (2.00), 369 (1.93), 399 (0.75), 448 (0.58)

The electronic absorption spectra of $[Ru(PPh_3)_2(BZM)_2Cl_2]$ in methanol generally showed two absorption bands in 550 to 450 nm range with ε of the order 10^3. The band around 550 nm in **MLS4** is weaker than that around 450 nm. The band around 550 nm may have some MLCT character and also certain amount of *d-d* character.

X-ray diffraction studies: Structural studies were carried out by powder X-ray diffraction using a 1.4 kW Cu-rotating anode based Rigaku (Tokyo, Japan) powder diffractometer operating in Bragg-Brentano geometry and fitted with a curved crystal graphite monochromator in the diffraction beam and a high temperature attachment. The XRD data in the 2θ range of 20-80º at a step of 0.02º were collected at room temperature. Fig. 1 depicts the XRD patterns of samples **MLS1**, **MLS2**, **MLS3**, **MLS4** and **MLS5**. It is evident that samples **MLS1**, **MLS2** and **MLS5** are stabilized in the crystalline form at room temperature. However samples **MLS3**, **MLS4** are most like amorphous in nature as no sharp Bragg′s peaks were observed. In order to investigate the crystal structure of the samples **MLS1**, **MLS2** and **MLS3**, Lebail profile fittings were carried out using FULLPROF package [28]. In present profile fittings, pseudo-Voigt function and a sixth order polynomial were used

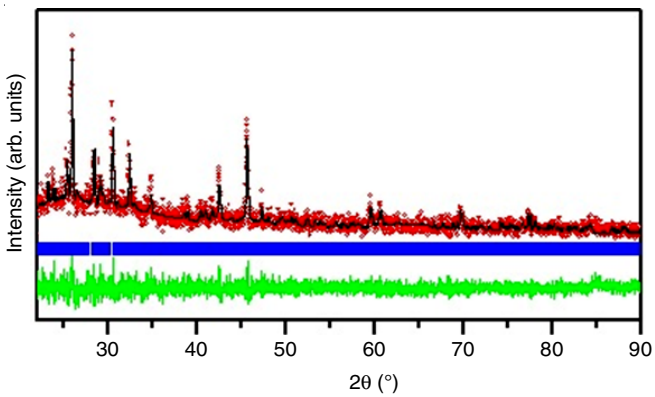

Fig. 1. X-Ray diffraction pattern of metal complex

to define the profile shape and background, respectively. During the profile fittings, parameters, such as the scale factor, zero correction, background, half-width parameters, the mixing parameters, lattice were varied. Table-2 depicts the observed, calculated and difference profiles obtained after the Lebail analysis of the full XRD pattern for **MLS2** using monoclinic space group P21/c. The fit between the observed and calculated profiles is quite good suggest that the sample **MLS5** most likely

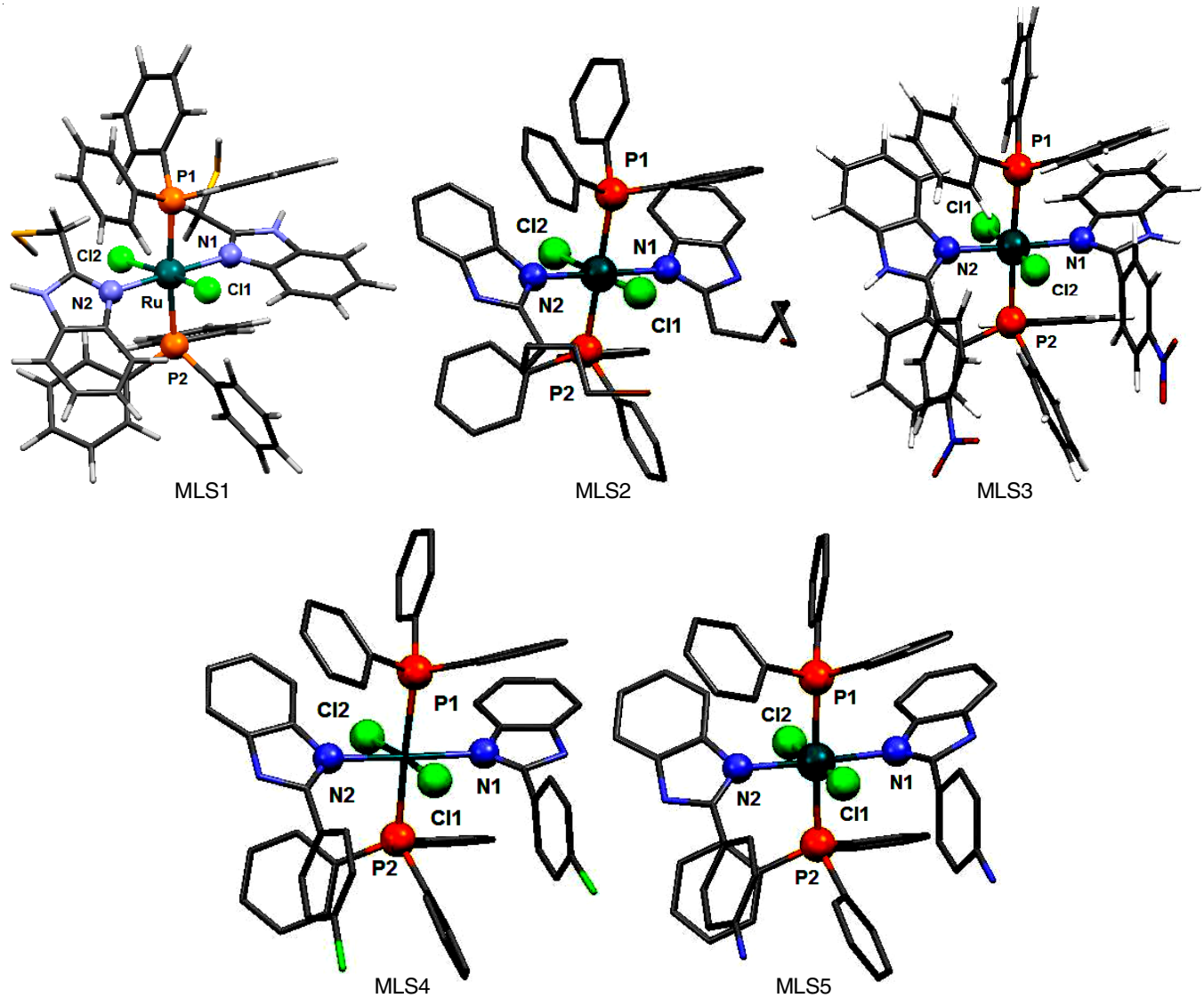

Fig. 2. Perspective view of optimized geometry of metal complexes

TABLE-2
UNIT CELL PARAMETER OBTAINED AFTER PROFILE FITTING OF X-RAY DIFFRACTION DATA COLLECTED AT ROOM TEMPERATURE USING MONOCLINIC SPACE GROUP p21/c

Sample	a (Å)	b (Å)	c (Å)	α (°)	β (°)	γ (°)
MLS1	17.521(2)	21.562(4)	10.719(1)	90.00	91.05(1)	90.00
MLS2	17.996(3)	22.086(5)	11.0178(2)	90.00	90.94(2)	90.00
MLS3	18.010(2)	22.076(3)	10.978(3)	90.00	91.01(1)	90.00

stabilized in the monoclinic phase at room temperature with space group P21/c symmetry. The unit cell parameters obtained after the Lebail profile fittings for the samples **MLS1**, **MLS2** and **MLS3** are given in Table-2.

Optimized geometry of complexes: In order to gain structural insight regarding the synthesized Ru(II) complexes, density functional theory (DFT) calculations were performed using suitable functional (vide infra). Perspective views of optimized geometry of these complexes have been presented in Fig. 2. The relevant optimized geometrical parameters of these complexes are comparable with the analogues Ru(II) complexes [19,29-32]. The geometry optimization results indicate that in all of the complexes, Ru(II) centre acquires the octahedral geometry. The peculiar feature that is being observed in all the optimized geometry is that two PPh_3 moieties adopts *trans*-position with respect to each other. This can be attributed to the inherent bulkiness associated with the PPh_3 ligand and also because of the relatively strong *trans* directing influence by chloro ligands [19]. The pertinent optimized geometrical parameters for the Ru(II) complexes is shown in Table-3.

TABLE-3
OPTIMIZED GEOMETRICAL PARAMETERS FOR Ru(II) COMPLEXES [BOND LENGTH (Å) AND BOND ANGLE (°)]

Parameter	MLS1	MLS2	MLS3	MLS4	MLS5
Ru-N1	2.230	2.319	2.330	2.268	2.314
Ru-N2	2.307	2.257	2.261	2.322	2.258
Ru-P1	2.529	2.515	2.511	2.552	2.551
Ru-P2	2.513	2.562	2.534	2.506	2.502
Ru-Cl1	2.513	2.510	2.534	2.472	2.502
Ru-cl2	2.541	2.543	2.473	2.539	2.427
Ru-N1-C	126.94	125.70	125.21	123.85	125.60
Ru-N2-C	126.72	125.85	123.81	125.19	122.25
Ru-P1-C	117.92	115.44	112.30	114.37	110.88
Ru-P2-C	122.52	124.21	123.07	117.53	123.61
P1-Ru-P2	174.45	177.53	176.40	176.19	177.42
Cl1-Ru-Cl2	170.63	176.78	175.47	175.21	177.57

Morphological cytotoxicity study: The morphological changes in HeLa cells were observed under inverted phase contrast microscope after treatment of **MR**, **MLS2** and **LS1** at 10, 25, 50, 100 and 200 µM concentrations for 24 h. As depicted in Fig. 3, severe changes were observed in the morphology of HeLa cells treated with **MR**, **MLS2** and **LS1**. The treated cells showed a typical feature of apoptosis *viz*. cytoplasmic vacuolization, cellular shrinkage, became round shape and nuclear condensation as compared to the untreated cells which were also reported by an earlier study [33]. While the untreated control cells exhibit even cell surface, flat and remained smooth, signifying the morphology of healthy cells.

Nuclear condensation and apoptosis: Induction of apoptosis in cancerous cells is considered as a valuable method to cure the various cancers. Apoptosis is usually characterized by

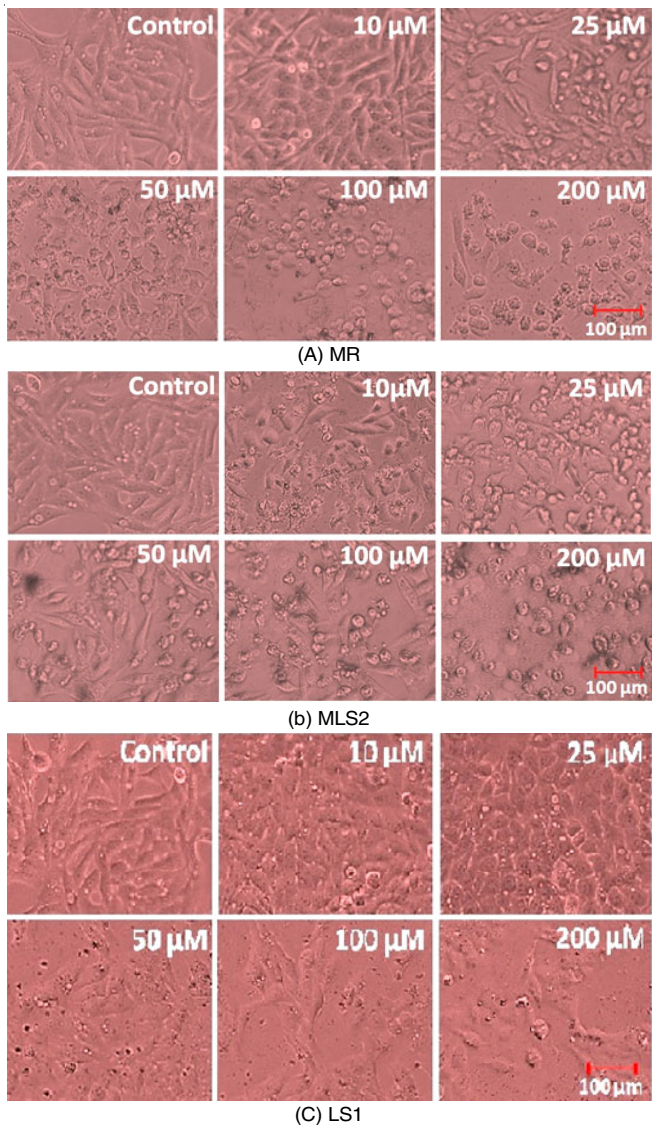

Fig. 3. Photomicrograph showing morphological changes in HeLa cells after treatment with 10, 25, 50, 100 and 200 µM concentrations of (A)MR (B)MLS2 and (C) LS1, at 24 h by inverted phase contrast microscopy

the typical morphological and biological changes in cells like shrinkage of the cell, condensation of nuclear chromatin and fragmented apoptotic bodies [34]. In this study, we observed concentration dependent nuclear apoptosis in HeLa cells in **MR**, **MLS2** and **LS1**. As evident from photomicrographs of HeLa cells (Fig. 4), synthesized compounds exhibit apoptosis in HeLa cells evident by the occurrence of chromatin condensation and nuclear bounded apoptotic bodies. As evident from the pictorial graph representing quantitative % apoptotic cells at 25, 50 and 100 µM of **MR** showed approximately 9.39, 16.347 and 23.34 % of apoptotic cells in HeLa cells. Furthermore, at

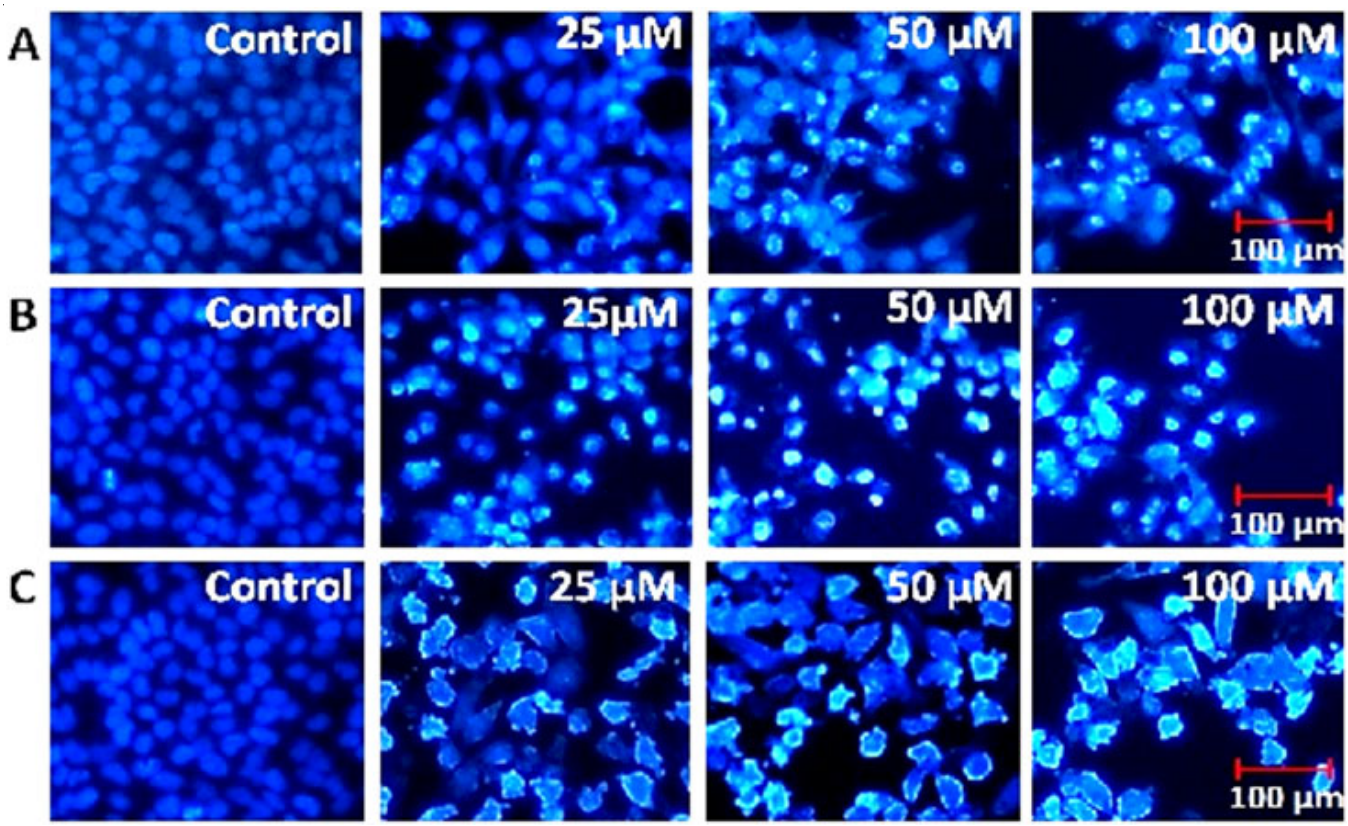

Fig. 4. Photomicrograph showing morphological changes, nuclear condensation and cellular apoptosis on HeLa cells, treated with 25, 50 and 100 µM of MR, MLS2 and LS1 against HeLa cells

25, 50 and 100 µM doses of **MLS2**, showed around 14.34, 21.85 and 30.67 % of apoptotic cells and **LS1** showed approximately 6.67, 12.34 and 20.85 % apoptotic cells with respect to control (Fig. 5). The photomicrograph of HeLa cells having condensed and fragmented nuclei suggest that **MR**, **MLS2** and **LS1** induced the cell death by the process of apoptotic. The anti-proliferative effects of **MR**, **MLS2** and **LS1** on HeLa cells were inspected using the MTT assay after 24 h exposure. As revealed from Fig. 6, data of cell viability on HeLa cells displayed that **MR** at 10, 25, 50, 100 and 200 µM concentrations significantly reduced the viability 92.01, 79.18, 63.99, 52.31 and 39.18 % ($p < 0.001$) respectively, as compared to untreated cells (taken as 100 % viable). Likewise at 10, 25, 50, 100 and 200 µM doses

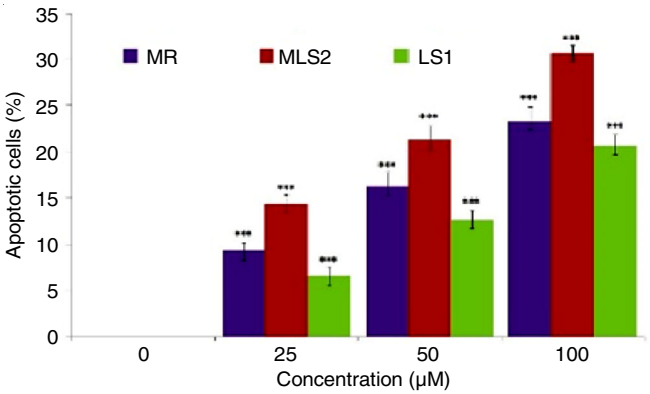

Fig. 5. Column graph representing % apoptotic cells in HeLa cells at 25, 50 and 100 µM concentrations of MR, MLS2 and LS1. Data were represented as mean ± SEM of three independent experiments and value of p*** ≤ 0.001

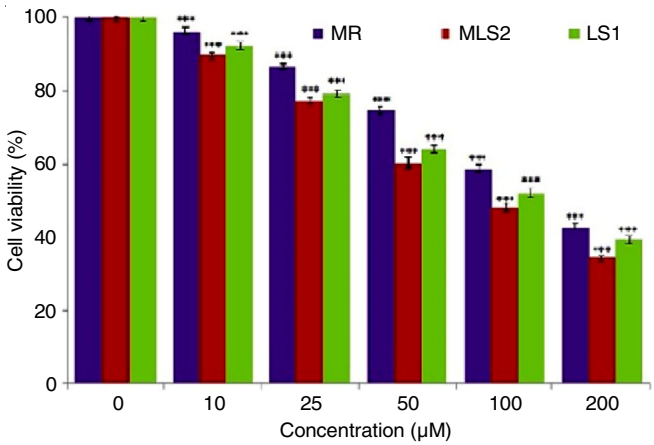

Fig. 6. Column graph demonstrating as the % cell viability at different concentrations of MR, MLS2 and LS1on HeLa cells, calculated by MTT assay after 24 h incubation. Data are represented as mean ± SEM of three independent experiments and value of p*** ≤ 0.001

of **MLS2** treatment reduced the cell viability in 89.43, 77.01, 60.00, 47.87 and 34.37 %, while **LS1** showed approximately 96.21, 86.38, 74.40, 58.87 and 42.79 % ($p < 0.001$) reduction of viable cells, with respect to the control. The results clearly recommended that **MR**, **MLS2** and **LS1** significantly reduced the viability of cervical carcinoma cell line depending upon dose. The IC_{50} value of **MR**, **MLS2** and **LS1** against HeLa cells was estimated to be 90.8, 81.8 and 115 µg/mL, respectively and suggested that **MLS2** was found to be more toxic as compared to **MR** and **LS1**. This study also supported the previous report that metal complexes were more toxic than that of ligand [35].

Intracellular ROS generation: The apoptosis is characterized by drastic alterations in expression and action of some potent apoptotic markers [36]. ROS production has also been involved in an initial incident of the cellular apoptosis and various cancer chemotherapeutic drugs induce apoptosis by induction of ROS [36]. Present result also supports the ROS-mediated cellular apoptosis in HeLa cells with the increasing concentrations of **MR**, **MLS2** and **LS1** as compared to untreated cells (Fig. 4). Similarly, the results obtained from the quantitative fluorescence intensities showed that 25 µM concentration of **MR**, **MLS2** and **LS1** induced ROS production approximately 119.56,125.19 and 108.95 % (***$p < 0.001$), respectively as compared to control. At 50 µM concentration of **MR**, **MLS2** and **LS1** increased by nearly 127.67, 140.48 and 119.38 % (***$p < 0.001$), respectively, whereas the maximum ROS level approximately 147.07, 167.79 and 135.21 % (***$p < 0.001$), were observed at the concentrations of 100 µM when compared to untreated cells (Fig. 7). As depicted from the result of DCF fluorescence the compound **MLS2** found to be more toxic with respect to **MR** and **LS1**. The conclusion of present study provides a supportive molecular mechanism of cellular apoptosis of the tested **MR**, **MLS2** and **LS1**.

Conclusion

The cellular apoptosis by MTT assay proposed that **MR**, **MLS2** and **LS1** significantly reduced the viability of HeLa cells in a dose-dependent manner. The inhibitory concentration (IC_{50}) value of **MR**, **MLS2** and **LS1** was estimated to be 90.8, 81.8 and 115 µg/mL for HeLa cells, respectively. The excessive ROS generation supports the molecular mechanism of apoptosis as well as the data of nuclear condensation assay, also suggested that these synthesised compound induced cell death in HeLa cells by an apoptotic manner.

ACKNOWLEDGEMENTS

The authors gratefully acknowledge Rajiv Gandhi National Fellowship for financial Support and DST-PURSE, Department of Chemistry, Lucknow University, Lucknow, India.

CONFLICT OF INTEREST

The authors declare that there is no conflict of interests regarding the publication of this article.

REFERENCES

1. B. Rosenberg, L. Van Camp, J.E. Trosko and V.H. Mansour, *Nature*, **222**, 385 (1969); https://doi.org/10.1038/222385a0.
2. L. Kelland, *Nat. Rev. Cancer*, **7**, 573 (2007); https://doi.org/10.1038/nrc2167.
3. S. Medici, M. Peana, V.M. Nurchi, J.I. Lachowicz, G. Crisponi and M.A. Zoroddu, *Coord. Chem. Rev.*, **284**, 329 (2015); https://doi.org/10.1016/j.ccr.2014.08.002.
4. A. Bergamo, C. Gaiddon, J.H. Schellens, J.H. Beijnen and G. Sava, *J. Inorg. Biochem.*, **106**, 90 (2012); https://doi.org/10.1016/j.jinorgbio.2011.09.030.
5. J.M. Rademaker-Lakhai, D. van den Bongard Pluim, J.H. Beijnen and J.H.M. Schellens, *Clin Cancer Res.*, **10**, 3717 (2004); https://doi.org/10.1158/1078-0432.CCR-03-0746.
6. M. Brindell, I. Stawoska, J. Supel, A. Skoczowski, G. Stochel and R. van Eldik, *J. Biol. Inorg. Chem.*, **13**, 909 (2008); https://doi.org/10.1007/s00775-008-0378-3.
7. C.G. Hartinger, S. Zorbas-Seifried, M.A. Jakupec, B. Kynast, H. Zorbas and B.K. Keppler, *J. Inorg. Biochem.*, **100**, 891 (2006); https://doi.org/10.1016/j.jinorgbio.2006.02.013.
8. A.K. Singh, G. Saxena, Sahabjada and M. Arshad, *Specrochim. Acta A: Mol. Biomol. Spectrsc.*, **180**, 97 (2017); https://doi.org/10.1016/j.saa.2017.02.056.
9. A.K. Singh, G. Saxena, S. Dixit, S.K. Hamidullah, S.K. Singh, S.K. Singh, M. Arshad and R. Konwar, *J. Mol. Struct.*, **1111**, 90 (2016); https://doi.org/10.1016/j.molstruc.2016.01.070.
10. A.H. Cory, T.C. Owen, J.A. Barltrop and J.G. Cory, *Cancer Commun.*, **3**, 207 (1991); https://doi.org/10.3727/095535491820873191.
11. P.J. Dyson, *Chimia*, **61**, 698 (2007); https://doi.org/10.2533/chimia.2007.698.
12. R. Palchaudhuri and P.J. Hergenrother, *Curr. Opin. Biotechnol.*, **18**, 497 (2007); https://doi.org/10.1016/j.copbio.2007.09.006.
13. G. Stochel, A. Wanat, E. Kulis and Z. Stasicka, *Coord. Chem. Rev.*, **171**, 203 (1998); https://doi.org/10.1016/S0010-8545(98)90033-9.
14. H. Miki, N. Uehara, A. Kimura, T. Sasaki, T. Yuri, K. Yoshizawa and A. Tsubura, *Int. J. Oncol.*, **40**, 1020 (2012); https://doi.org/10.3892/ijo.2012.1325.
15. T.M. Li, G.W. Chen, C.C. Su, J.G. Lin, C.C. Yeh, K.C. Cheng and J.G. Chung, *Anticancer Res.*, **25**, 971 (2005).
16. S. Siddiqui, E. Ahmad, M. Gupta, V. Rawat, N. Shivnath, M. Banerjee, M.S. Khan and M. Arshad, *Cell Prolif.*, **48**, 443 (2015); qhttps://doi.org/10.1111/cpr.12195.
17. R.K. Singh, A.K. Singh, S. Siddiqui, M. Arshad and A. Jafri, *J. Mol. Struct.*, **1135**, 82 (2017); https://doi.org/10.1016/j.molstruc.2017.01.059.
18. G. Mariappan, R. Hazarika, F. Alam, R. Karki, U. Patangia and S. Nath, *Arab. J. Chem.*, **8**, 715 (2015); https://doi.org/10.1016/j.arabjc.2011.11.008.
19. T.A. Stephenson and G. Wilkinson, *J. Inorg. Nucl. Chem.*, **28**, 945 (1966); https://doi.org/10.1016/0022-1902(66)80191-4.
20. P.S. Hallman, T.A. Stephenson and G. Wilkinson, *Inorg. Synth.*, **12**, 40 (1970); https://doi.org/10.1002/9780470132432.ch40.
21. S. Sabo-Etienne and M. Gellier, Encyclopedia of Inorganic Chemistry, John Wiley & Sons (2006).
22. A.D. Becke, *J. Chem. Phys.*, **98**, 5648 (1993); https://doi.org/10.1063/1.464913.
23. J.P. Perdew and Y. Wang, *Phys. Rev. B*, **45**, 13244 (1992); https://doi.org/10.1103/PhysRevB.45.13244.
24. A.M. Pyle, J.P. Rehmann, R. Meshoyrer, C.V. Kumar, N.J. Turro and J.K. Barton, *J. Am. Chem. Soc.*, **111**, 3051 (1989); https://doi.org/10.1021/ja00190a046.
25. R. Lalrempuia, P.J. Carroll and M.R. Kollipara, *J. Coord. Chem.*, **56**, 1499 (2003); https://doi.org/10.1080/00958970310001628957.
26. P. Sengupta, S. Ghosh and T.C.W. Mak, *Polyhedron*, **20**, 975 (2001); https://doi.org/10.1016/S0277-5387(01)00736-7.
27. S.A. Moya, R. López, C. Pérez-Zúñiga, M. Yáñez and P. Aguirre, *J. Coord. Chem.*, **68**, 2423 (2015); https://doi.org/10.1080/00958972.2015.1047357.
28. R. Karvembu and K. Natarajan, *Polyhedron*, **21**, 1721 (2002); https://doi.org/10.1016/S0277-5387(02)01038-0.
29. J. Rodríguez-Carvajal, *Physica B*, **192**, 55 (1993); https://doi.org/10.1016/0921-4526(93)90108-I.
30. J. Yellol, S.A. Pérez, A. Buceta, G. Yellol, A. Donaire, P. Szumlas, P.J. Bednarski, G. Makhloufi, C. Janiak, A. Espinosa and J. Ruiz, *J. Med. Chem.*, **58**, 7310 (2015); https://doi.org/10.1021/acs.jmedchem.5b01194.
31. S. Chowdhury, A. Bhattacharya, P. Saha, S. Majumder, E. Suresh and J.P. Naskar, *J. Coord. Chem.*, **69**, 3664 (2016); https://doi.org/10.1080/00958972.2016.1234047.
32. B.J. Coe, M. Helliwell, J. Raftery, S. Sánchez, M.K. Peers and N.S. Scrutton, *Dalton Trans.*, **47**, 5210 (2016); https://doi.org/10.1039/C5DT03753K.
33. D. J. Taatjes, B. E. Sobel and R. C. Budd, *Histochem. Cell. Biol.*, **129**, 33 (2008).
34. M. Arshad, S. Siddiqui and D. Ali, *Caryologia*, **69**, 128 (2016); https://doi.org/10.1080/00087114.2015.1136542.
35. G.I. Evan and K.H. Vousden, *Nature*, **411**, 342 (2001); https://doi.org/10.1038/35077213.
36. M. Chen, B. Zhou, P. Zhong, V. Rajamanickam, X. Dai, K. Karvannan, H. Zhou, X. Zhang and G. Liang, *Prostate*, **77**, 489 (2017); https://doi.org/10.1002/pros.23287.